Arabian Journal of Chemistry (2021) **14**, 103453

King Saud University

Arabian Journal of Chemistry

www.ksu.edu.sa
www.sciencedirect.com

ORIGINAL ARTICLE

Isotherms, kinetics, and thermodynamics of boron adsorption on fibrous polymeric chelator containing glycidol moiety optimized with response surface method

Haruna Kolawole Afolabi [a,*], Mohamed Mahmoud Nasef [b,*], Nik Abdul Hadi Md Nordin [a,*], Teo Ming Ting [c], Noorfidza Yub Harun [a], Anwar Ameen Hezam Saeed [a]

[a] *Chemical Engineering Department, Universiti Teknologi PETRONAS, Seri Iskandar 32610, Malaysia*
[b] *Malaysia-Japan International Institute of Technology, Universiti Teknologi Malaysia, Jalan Sultan Yahya Petra, 54100 Kuala Lumpur, Malaysia*
[c] *Radiation Processing Technology Division, Malaysian Nuclear Agency, 43000 Kajang, Selangor, Malaysia*

Received 20 August 2021; accepted 21 September 2021
Available online 29 September 2021

KEYWORDS

Polyvinylamine grafted PE/PP;
Fibrous polymeric chelator;
Boron-selective adsorption;
Glycidol density;
Box-Behnken design

Abstract A fibrous boron chelator containing glycidol moiety (PE/PP-*g*-PVAm-G) was prepared by radiation induced grafting of N-vinylformamide (NVF) onto polyethylene/polypropylene (PE/PP) non-woven sheet followed by hydrolysis and immobilization of glycidol moiety. The glycidol density was controlled by optimization of the reaction parameters using the Box-Behnken design of response surface methodology (RSM). The properties of the PE/PP-*g*-PVAm-G were evaluated using Fourier transform infrared (FTIR) spectroscopy, field emission scanning electron microscopy (FESEM) and energy dispersive x-ray (EDX) analysis, X-ray diffraction (XRD) and thermal gravimetric analysis (TGA). A maximum glycidol density yield of 5.0 mmol·g^{-1} was obtained with 11.8 vol%, 78.9 °C and 109.4 min for glycidol concentration, reaction temperature and time, respectively. The isotherms, kinetics, and thermodynamic behavior of boron adsorption on the optimized chelator were investigated. The boron adsorption was pH-dependent and attained a maximum adsorption capacity of 25.7 mg·g^{-1}. The equilibrium isotherm proceeded by Redlich–Peterson

* Corresponding authors.
E-mail addresses: haruna_18002856@utp.edu.my (H.K. Afolabi), mahmoudeithar@cheme.utm.my (M.M. Nasef), nahadi.sapiaa@utp.edu.my (Nik Abdul Hadi Md Nordin).

Peer review under responsibility of King Saud University.

ELSEVIER Production and hosting by Elsevier

https://doi.org/10.1016/j.arabjc.2021.103453

model whereas the kinetics was best expressed by the pseudo-second-order equation. The thermodynamic analysis revealed that boron adsorption is endothermic and spontaneous. The fibrous chelator demonstrated high boron selectivity and strong resistance to foreign ions with uncompromised regeneration efficiency after five adsorption/desorption cycles. The PE/PP-*g*-PVAm-G chelator seems to be very promising for boron removal from aqueous media.

1. Introduction

Boron is a pollutant to surface, ground and wastewater that has been subjected to various decontamination investigations. Boron has never been elementally found in nature, but it is instead naturally existing in form of complex compounds of sodium or calcium borates such as tinkal ($Na_2O.2B_2O_3{\cdot}10H_2O$), ulexite ($Na_2O.2CaO.5B_2O_3{\cdot}16H_2O$) and colemanite ($2CaO.3B_2O_3{\cdot}5H_2O$) and its concentration in different water bodies is in the range of 5–100 ppm. The rise in boron pollution is caused by the widespread use of its compounds in industrial operations for borosilicate glass, ceramic glazes, porcelain enamels, pharmaceutical products, pesticides, and agricultural markets (Ezechi et al., 2012; Lin et al., 2021; Tang et al., 2017a, b). The leakage of boron to different water bodies poses very serious environmental problems and toxic effects to humans, plants, and animals. Boron limits for agricultural water is set between 0.3 and 1 ppm and that of drinking water stands maximally at 2.4 ppm according to WHO, whereas that of wastewater was set to few milligrams per liter depending on disposal regulations in various countries (Ezechi et al., 2012; Güler et al., 2015; Herschy, 2012; Wolska and Bryjak, 2013). Thus, effective boron removal methods are in high demand for wastewaters de-boronation to meet the environmental regulations and wastewater disposal standards.

Currently, there is no unique technique to satisfactorily remove boron from wastewater (Recepoğlu et al., 2018), and practiced methods include chemical precipitation (B. Wang et al., 2014), nanofiltration (Landi et al., 2019), reverse osmosis (Zhe Wang et al., 2021), electro-deionization, electrodialysis (Ezechi et al., 2012), electrocoagulation (Chen et al., 2020), and ion-exchange (Ezechi et al., 2012; Güler et al., 2015; Kabay et al., 2008; Najid et al., 2021). Among all, ion-exchange method is one of the most appealing methods for effective removal of boron from wastewater to low concentrations conforming to guidelines and disposal criteria around the world (Dydo and Turek, 2013). This technique relies on the selective ability of *N*-methyl-*D*-glucamine (NMDG)-containing resins having multiple alcoholic hydroxyl groups that react with borate to form chelate complexes (Ince et al., 2013). Its operational requirements are quite simple, and it's mostly applicable to solutions with lower boron concentrations. The chemistry of boron has shown that polymers bearing molecules with vicinal diols (e.g. glucamine or glycidol functionality) have the ability to bind boric acid by forming either neutral boron esters or borate type of complex compounds in aqueous solutions by esterification reaction (Kamcev et al., 2019; Sanfeliu et al., 2018). As a result, partial esterification could result in mono-chelate of 1:1 boron: polyol complexes while complete esterification may create a bis-chelate 1:2 boron: polyol complexes in Fig. 1. The former complex is labile and quickly hydrolyzed to their original components in solution, whereas the later is indissociable and much more thermodynamically stable in water (Kamcev et al., 2019; Sanfeliu et al., 2018). However, these resins are challenged by some drawbacks such as slow kinetics, considerable loss in capacity after regeneration by acid treatment and are economically costly.

Exploration of new chelating adsorbents (boron chelator) with better properties and performance toward the selectivity of boron is imperative. Surface modification of polymeric substrates by graft copolymerization has been frequently used to incur NMDG moieties to develop alternative boron selective chelators with improved chemical and structural properties. Notably, fibrous polymeric chelators with NMDG prepared by radiation induced graft copolymerization (RIGC) have demonstrated improved properties and higher boron chelation performance compared to granular commercial resins (Hoshina et al., 2021; Ting et al., 2020). This is due to their higher functional group density and the associated higher wettability in boron solutions allowing not only stronger affinity and enhanced diffusion but also rapid interaction of boron

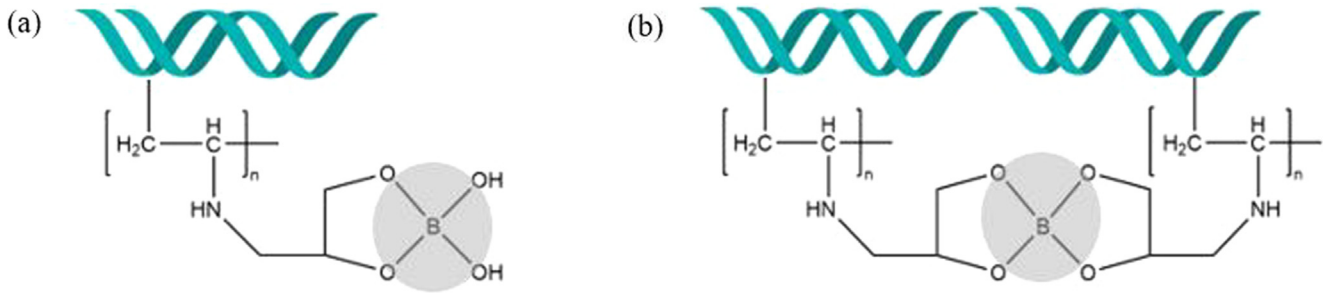

Fig. 1 Schematic mechanism representation of: (a) mono-chelate and (b) bis-chelate ester complex formed during boron adsorption on glycidol-containing adsorbent.

with functional groups (Nasef et al., 2014; Recepoğlu et al., 2017; Recepoğlu et al., 2018; Tang et al., 2017a). Nonetheless, the performance of NMDG is still not satisfactory and there is room to improve the adsorption capacity and the kinetics by incorporation of alternative functional groups such as glycidol.

Glycidol is an alternative weakly basic moiety that has been used to prepare boron chelating adsorbents based on substrates of various morphologies that started to receive attention in the past several years as indicated in the summary of previous studies depicted in Table 1 (Luo et al., 2020a; Senkal and Bicak, 2003; Zerze et al., 2013). Particularly, boron polymeric chelators including poly(glycidyl methacrylate (GMA)–methyl methacrylate (MMA)–DVB (divinylbenzene) beads (Senkal and Bicak, 2003), poly(GMA/trimethylolpropane trimethacrylate) nano-beads (Luo et al., 2020a), crosslinked poly (N-vinylformamide) (NVF) microporous beads (Ince et al., 2013), polysulfone membrane (Jin et al., 2019), poly[N-(2,3-dihydroxypropyl)aminostyrene] beads (Nesterov et al., 2013), polyacrylonitrile membrane (Meng et al., 2016), magnetic chitosan microbeads with *cis*-diols (Oladipo and Gazi, 2016), and microporous DVB cross-linked polystyrene resin (Kluczka et al., 2015), modified with different amine ligands to host glycidol were investigated. Despite such contributions, fibrous polymeric chelators functionalized with glycidol ligands are rarely reported. It was recently our research group explored the preparation of fibrous chelator and its potential application for boron removal for aqueous solution (Afolabi et al., 2021a). PE/PP is a versatile substrate with PE sheath and PP core chosen as inert polymer for the development of fibrous adsorbent with strong radiation resistance, high mechanical integrity with chemical stability, and low cost. The polymeric chelator was prepared by RIGC of NVF onto PE/PP nonwoven sheet followed by hydrolysis of amide to amine and subsequent incorporation of glycidol ligands. However, neither optimization of glycidol content in the chelator nor isothermal, kinetics and thermodynamic behavior of the adsorption were investigated.

To enhance the performance, sustainability, and economy of the reaction, the density of the glycidol must be maximized through optimization of functionalization reaction. This can be carried out using response surface methodology (RSM) which is a combination of mathematical and statistical methods allowing the investigation of various independent variables effects on a dependent variable taking interactive effects of variables on the process performance. Furthermore, RSM enables the development of empirical models and helps in minimizing the number of experiments as well as the use of chemicals, expensive analysis, and time which in turn reduces the costs (Bezerra et al., 2008; Melo et al., 2020). Thus, optimization studies pertaining to the incorporation of functional groups into the chelator precursors to enhance their performance in water and wastewater treatments become appealing (Melo et al., 2020; Moawia et al., 2019; Nallappan et al., 2018).

The objective of this article is to optimize the glycidol immobilization reaction conditions to maximize the glycidol density and to investigate the isotherms, kinetics, and thermodynamics of boron adsorption of the new fibrous chelator. Box Benkhen Design (BBD) in response surface methodology was applied to study the effect of various reaction parameters such as glycidol concentration, reaction time and temperature on the glycidol density. The optimum values for obtaining the maximum glycidol density were determined and the performance was evaluated on batch basis. The adsorption mechanism was also elaborated.

2. Materials and methods

PE/PP non-woven fibrous sheets were procured from Kurashiki Co., Japan. Glycidol (96%) and NVF monomer (98%) were purchased from Sigma Aldrich (Saint Louis, MO, USA). Boric acid, hydrochloric acid (37%), sodium hydroxide and toluene were obtained from Merck (Darmstadt, Germany). Sulfuric acid of 95 to 98% was purchased from

Table 1 Summary of previous studies on preparation of glycidol containing boron chelating adsorbents.

Methods of preparation	Substrates	Monomers	Precursors	q_e ($mg \cdot g^{-1}$)	Refs
Polymerization	Nano-polymer beads	GMA/ trimethylolpropane trimethacrylate	Triethylenetetramine, ethylenediamine	23.3 29.2	(Luo et al., 2020b)
Co-deposition, functionalization	Polysulfone membrane	–	Dopamine, polyethyleneimine	17.4	(Jin et al., 2019)
Polymerization	Microspheres bead	NVF, DADMAC	Polyvinylamine	43.2	(Ince et al., 2013)
Polymerization	Terpolymer beads	GMA	Ethylenediamine	32.4	(Senkal and Bicak, 2003)
Hydrolysis, amidation	Polyacrylonitrile membrane	–	Hyperbranched polyethylenimine	34.6	(Meng et al., 2016)
Chemical modification	Microporous DVB cross-linked polystyrene resin with amine functional groups	–	Aminostyrene	1.6	(Kluczka et al., 2015)
Nitration, reduction, and functionalization	Poly[N-(2,3-dihydroxypropyl) aminostyrene]	–	Aminostyrene	–	(Nesterov et al., 2013)
Polymerization, hydrolysis, functionalization	Polyethylene/polypropylene	NVF	Polyvinylamine	21.4	(Afolabi et al., 2021b)

N-vinyl formamide = NVF, Glycidyl-methacrylate = GMA, Diallyldimethylammonium chloride (DADMAC).

R&M chemicals. Hach (Loveland, USA) provided the Boro-Ver®3 boron reagent powder kit. Deionized water (DI) obtained from the Barnstead nanopores diamond lab water purification system (Thermo Fisher, Waltham, USA) was used for washing and preparation of all solutions. All solvents were reagent grade, and they were used as received.

2.1. Synthesis of PE/PP-g-PVAm-G chelator

Radiation induced grafting was used to modify PE/PP non-woven sheet by placing the samples in PE zipped bags containing N_2 gas and sealed thermally. After that, the sample-containing bags were placed on dry ice before being irradiated with an electron beam accelerator (EPS 3000, Nissin High Voltage, Japan) at 25 kGy/pass with an absorbed dose of 300 kGy. The beam current was 10 mA, and the acceleration energy was 2 MeV. The samples irradiated were transferred into evacuated ampoules, and later filled with oxygen-free grafting solutions containing 20 vol% diluted NVF/toluene solution homogenized by bubbling. The ampoules were immersed in a thermostatic bath for a period of 3 h and reaction temperature of 70 °C for the grafting process. The grafted samples were taken from the ampoules and rinsed with methanol after the process a few times before being dried overnight under vacuum at 60 °C. The degree of grafting (DG) was gravimetrically estimated as 120 %. More details on RIG of NVF onto irradiated PE/PP non-woven sheets under various conditions can be found elsewhere in our previous publication (Afolabi et al., 2021a).

The grafted fibrous poly(N-vinyl formamide) (PNVF) chains in PE/PP sheets were hydrolyzed to polyvinylamine (PVAm) under reflux with 2 M solution of NaOH at 80 °C for 4 h in an oil bath. After the reaction, the treated sample was washed and dried at 60 °C under a vacuum oven. The amine content of the PVAm sample was determined by placing 0.5 g of the samples in 10 mL of 1 M HCl for 24 h. 2.5 mL from the residual acidic solution was titrated against 0.1 M NaOH solution in the presence of phenolphthalein (Senkal and Bicak, 2003). The total amine density was estimated as 5.13 mmol·g^{-1}.

2.2. Experimental design for glycidol immobilization

The PVAm chelator precursors were functionalized by dispersing the samples in DI water under stirring. Dropwise additions of glycidol were added to the mixture at room temperature along with continuous stirring before transferring to an oil bath heated at predetermined temperature and reaction time under reflux. The various reaction parameters were varied according to the experimental design for the purpose of optimization to determine the reaction condition with the best response. After the reaction, the samples were washed with an excess amount of DI water and oven-dried at 60 °C in a vacuum to constant weight. Fig. 2 shows a scheme for the grafting of NVF onto PE/PP non-woven sheet, followed by base hydrolysis and the immobilization of glycidol moiety into the PVAm chelator precursor.

Three variable process parameters viz; concentration of glycidol, reaction time and temperature were optimized using BBD with Design Expert software (Version 10.0.1.0, Stat-Ease, Inc., Minneapolis, USA) for statistical model formation. The yield which is referred to as the glycidol functional group density was set as the system response (dependent variable). The total number of experimental runs was 17 with three-coded levels -1, 0 and + 1 involving three independent variables used for the prediction of optimum yield. Table 2 shows the ranges of the experimental values of independent variables. The glycidol functional group density in PE/PP-g-PVAm-G was calculated with Eq. (1):

$$\text{Glycidol density } (\text{mmol.g}^{-1}) = \frac{W_f - W_I}{74.08\,W_f} \times 1000 \qquad (1)$$

where, the weight of the adsorbent precursor (PVAm) and final weight of functionalized glycidol-containing chelator are respectively represented by W_i and W_f. The figure 74.08 g·mol^{-1} is the molar mass of glycidol.

The experimental ranges selected for the independent variables were 5−15 vol% of glycidol concentration, 60−80 °C for reaction temperature and 1−2 h of reaction time. The independent variables and experiment data from response surface analysis are presented in Table 3. The application of the p-value test to experimental results was used for the establishment of whether the parameter is significant to a 95% level

Table 2 Three-coded level for the variable process parameters used.

Terms	Design variables	Units	Coded levels		
			−1	0	1
A	Glycidol concentration	vol %	5	10	15
B	Reaction temperature	°C	60	70	80
C	Reaction time	h	1	1.5	2

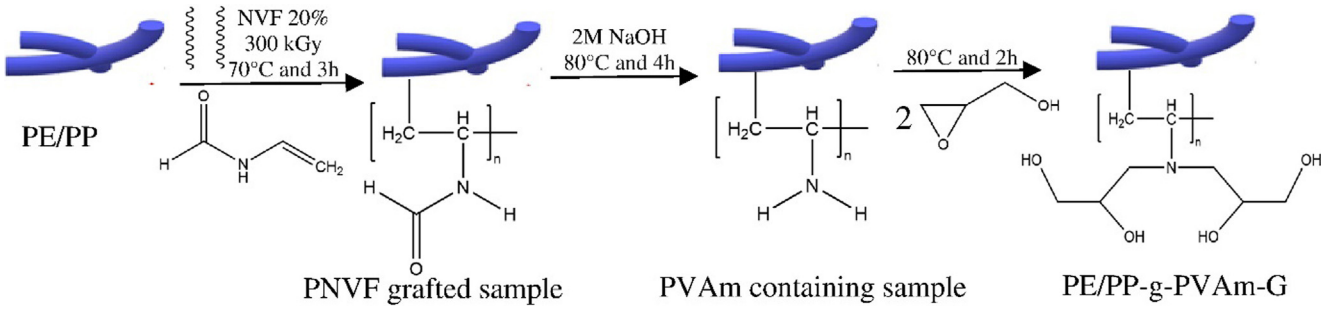

Fig. 2 Synthesis scheme for the grafting of NVF onto PE/PP non-woven fiber sheet, base hydrolysis, and the immobilization of glycidol.

Table 3 Response surface analysis independent variables and experiment results.

Std	Run	A:Concentration (Vol %)	B:Temperature (°C)	C:Time (h)	Functional group density (mmol·g^{-1})	
					Actual	Predicted
5	1	5	70	1	2.09	2.09
2	2	15	60	1.5	3.36	3.40
7	3	5	70	2	2.88	2.98
4	4	15	80	1.5	4.77	4.83
3	5	5	80	1.5	3.89	3.85
6	6	15	70	1	3.25	3.15
13	7	10	70	1.5	3.89	3.96
11	8	10	60	2	3.39	3.35
1	9	5	60	1.5	1.56	1.50
16	10	10	70	1.5	3.91	3.96
15	11	10	70	1.5	4.02	3.96
17	12	10	70	1.5	4.09	3.96
10	13	10	80	1	3.94	3.98
12	14	10	80	2	5.03	4.97
9	15	10	60	1	1.75	1.81
8	16	15	70	2	4.78	4.78
14	17	10	70	1.5	3.88	3.96

of confidence. The predicted and corresponding experimental values of glycidol functional group density were compared. For the purpose of validating the model adequacy with the experimental data, the analysis of variance (ANOVA) was used. The determination coefficients R^2, adjusted R^2 and predicted R^2 from the analysis were estimated to check the model developed. Consequently, the values predicted by the equation developed from the model were compared with the verification experiments performed at optimum conditions. The independent variables interactions and their corresponding influence on the glycidol functional group density were examined using three-dimensional (3D) response surface plots.

2.3. Characterization of PE/PP-g-PVAm-G chelator

The crystallinity and structural properties of PE/PP-*g*-PVAm-G were analyzed using a Malvern PANalytical X'Pert3 powder diffractometer at 40 mA with a Cu anode material (Kα1 = 1.5406 A°, Kα2 = 1.5444 A°) in the Bragg's angle range of 5−50°. The chemical compositions of PE/PP-*g*-PVAm-G chelator samples were characterized using Fourier transform infrared (FTIR) spectrophotometer (Nicolet Magna IR-750 spectrometer) composed of diamond ATR with a wavelength ranging from 650 to 4000 cm^{-1}. Field emission scanning electron microscopy (FESEM) was used to determine the morphology using Zeiss Supra 55 VP instrument and energy dispersive x-ray (EDX) spectrometer by Zeiss model EVO LS15 VPSEM was used to provide evidence of the distribution of various elements in the chelator at 15 kV. Thermogravimetric analysis (TGA) was used to test the thermal stability of the chelator using the Mettler Toledo TGA/SDTA 851e analyzer at a heating temperature range of 30–700 °C and a heating rate of 10 °C.

2.4. Batch adsorption experiment, isotherms, and kinetics studies

The adsorption properties of PE/PP-*g*-PVAm-G chelator were studied to assess its performance. A stock solution of boric acid was prepared in a plastic container by dissolving 5.716 g of H_3BO_3 in DI water and diluted to 1000 mL. Further solutions of desired concentrations (10−100 mgL^{-1}) were later freshly prepared for each experimental work. The effect of different pH of the solution on the adsorption of boron was evaluated in the range of 2−11 using 0.5 g of the adsorbent in 150 mL of 100 mg/L boric acid solution in plastic Erlenmeyer flasks and the solution is continuously shaken at 30 °C with a speed of 210 rpm. The adsorption isotherms and kinetics study were investigated with different concentrations of boron (10−100 mgL^{-1}) at a fixed fibrous chelator dose of 0.5 g in an Erlenmeyer flask containing 150 mL boric acid solution. The flask was shaken continuously at 210 rpm for 3 h in an incubator shaker. Few aliquots were withdrawn at predetermined time intervals and analyzed. The thermodynamic was studied in a similar condition at various temperatures (298 K, 303 K and 313 K). At the end of each experiment, the residual concentration of boron was spectrophotometrically determined at a wavelength of 610 nm using Shimadzu UV-2600 uv–visible spectrophotometer.

2.5. Analytical method

The boron concentration at equilibrium was measured using the carmine method. The procedure involves the addition of a BoroVer®3 reagent powder pillow into a 75 mL concentrated H_2SO_4 aqueous solution. The mixture was swirl for 5 min until the powder dissolves completely. 2 mL of the specimen and DI water were accurately pipetted into different 125 mL Erlenmeyer plastic flasks. In each flask, 35 mL of the prepared BoroVer®3/H_2SO_4 solution was added, swirled, and allowed to react for 30 min. The sample prepared was inserted into the cell holder of the UV–Vis spectrophotometer (Shimadzu UV-2600) at the wavelength of 610 nm. Eq. (2) was used for the estimation of the boron quantity at equilibrium q_e (mg/g).

$$q_e = [(C_o - C_e)V]/W \tag{2}$$

where, C_o and C_e represent the initial and final equilibrium concentrations of boron, respectively. V is the amount of volume used while W is the weight of dry fibrous chelator (g).

2.6. Boron adsorption in the presence of foreign ions

The effect of foreign ions on the adsorption properties of the boron fibrous chelator coexisting in a solution of Na^+, Ca^{2+}, Cl^- and SO_4^{2-} were studied. Aqueous solutions containing 300 mgL^{-1} of each ion and 0.5 g of PE/PP-*g*-PVAm-G chelator were added to 100 mgL^{-1} boric acids. The adsorption process was carried out for 3 h at 210 rpm. The quantity of boron adsorbed at equilibrium was then determined.

2.7. Re-usability of PE/PP-g-PVAm-G

The PE/PP-*g*-PVAm-G chelator was recovered by solvent desorption technique after the adsorption process. It was removed after the adsorption process from the solution and dipped into 1 M HCl solution to strip boron from the chelator, neutralized with 1 M NaOH and water washed. The regenerated PE/PP-*g*-PVAm-G was then re-applied for the adsorption process. The re-usability efficiency (RE%) was determined according to Eq. (3):

$$RE(\%) = \frac{q_{reg}}{q_{ori}} \times 100\% \quad (3)$$

where the q_{reg} ($mg{\cdot}g^{-1}$) is the boron adsorption capacity of the predetermined regeneration adsorption capacity, and q_{ori} ($mg{\cdot}g^{-1}$) is the original boron adsorption capacity of the fibrous chelator.

3. Results and discussion

3.1. Fitness of experimental data to model

A mathematical model was developed and analyzed from the experimental data fitted in the software. The BBD analysis used for testing the fitness of the model indicated that the quadratic and linear models were statistically significant with the p-value < 0.0001 while the cubic model was found to be aliased and could not be used for modeling as shown in Table 4. Hence, in this study the quadratic model was selected due to its good R^2 values (R^2 = 0.9954, adjusted R^2 = 0.9895 and predicted R^2 = 0.9573) suggested. The final equation of the model explaining the mathematical interaction between the three independent variables: A, B and C with the response in the range of the experimental data is represented by Eq. (4).

$$Y = +3.96 + 0.72A + 0.95B + 0.63C - 0.23AB + 0.19AC - 0.14BC - 0.42A^2 - 0.14B^2 - 0.29C^2 \quad (4)$$

where Y is the functional group density of glycidol, and A, B, and C represent the concentration of glycidol, reaction temperature, and reaction time, respectively.

3.2. Statistical analysis

The application of the ANOVA analysis was carried out to evaluate the response surface of the quadratic model and for the determination of the model significance as well as the individual term involved with respect to their p-values. The F-value of the model (169.28) suggests that the model is significant, with only a 0.01 percent chance of this F-value could occur due to noise. Consequently, the high F-value and low Prob > F value 0.0001 give an indication of Fisher's variance ratio significance as well as confirmation of the quadratic model with a high degree of fitness. Table 5 shows that the various terms A, B, C, AB, AC, BC, A^2, B^2, and C^2 from the model were significant because their Prob > F is < 0.0500. The "lack of fit" F-value (1.56) implies that this factor is not significant. There is a good correlation between the predicted and adjusted R^2 value while the Adeq precision for measuring the signal to noise ratio of the model is 49.442, suggesting that it can be utilized for navigation of the design space. Thus, these results show that the quadratic model predicted is in good agreement with the responses from the experimental and can therefore be adopted.

The ANOVA data was used to check the normality of the residuals as well as the predicted and actual responses as illustrated in Fig. 3. The plot of normal probability against the studentized residuals in Fig. 3a shows a linear trend which indicates the error distribution. As such, the model can be said to adequately predict the responses based on the reaction parameters. On the other hand with Fig. 3b showing the plot of predicted value indicate the appropriateness of the model and proper data dispersion (Nallappan et al., 2018).

3.3. Effects of independent variables and analysis of response surfaces

The interactions between the independent variables (concentration of glycidol, temperature, and reaction time) and glycidol's functional density in the fibrous chelator are represented by Fig. 4 as established by the ANOVA analysis. The numerical optimization technique of RSM was used to optimize the variables. The 3D plot of the response surface in Fig. 4a shows the variation of glycidol density with the concentration of glycidol and temperature at a constant reaction time of 90 min. An increase in the concentration of glycidol and reaction temperature results in an increase in glycidol density. A maximum glycidol density was achieved at a concentration of 12.85 vol% and a temperature of 80 °C, respectively. This observation can be ascribed to the temperature-enhanced diffusion of the glycidol moiety into the PVAm fibrous chelator precursor. The 3D surface plot for glycidol density versus reaction time and concentration at a constant temperature of 80 °C is presented in

Table 4 The model aptitude test for the response.

Source	Sequential p-value	Lack of Fit p-value	R-Squared	Adjusted R-Squared	Predicted R-Squared	
Linear	< 0.0001	0.0043	0.8900	0.8646	0.8194	
2FI	0.4178	0.0037	0.9161	0.8658	0.7751	
Quadratic	< 0.0001	0.3307	0.9954	0.9895	0.9573	Suggested
Cubic	0.3307		0.9979	0.9916		Aliased

Table 5 The ANOVA for response surface quadratic model to produce PE/PP-*g*-PVAm-G.

Source	Sum of Squares	DF	Mean Square	F-Value	Prob > F	Remarks
Model	16.18	9	1.80	169.28	< 0.0001	Significant
A-Concentration	4.12	1	4.12	387.72	< 0.0001	
B-Temperature	7.16	1	7.16	674.36	< 0.0001	
C-Time	3.19	1	3.19	300.11	< 0.0001	
AB	0.21	1	0.21	19.92	0.0029	
AC	0.14	1	0.14	12.89	0.0089	
BC	0.076	1	0.076	7.12	0.0321	
A^2	0.74	1	0.74	70.01	< 0.0001	
B^2	0.086	1	0.086	8.08	0.0250	
C^2	0.35	1	0.35	32.82	0.0007	
Residual	0.074	7	0.011			
Lack of Fit	0.040	3	0.013	1.56	0.3307	Not significant
Pure Error	0.034	4	8.570E-003			
Cor Total	16.26	16				

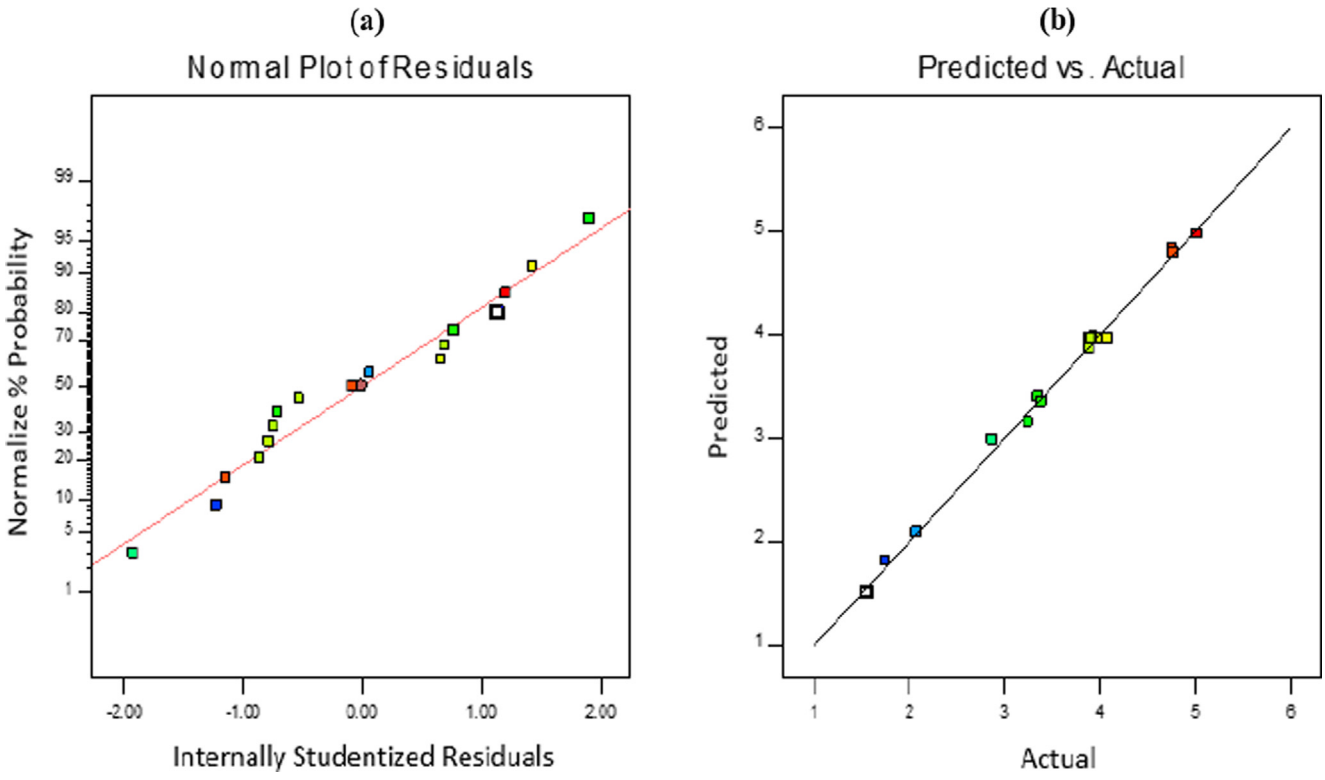

Fig. 3 Plot of (a) normal probability vs. studentized residuals and (b) predicted vs. actual numbers of response.

Fig. 4b. Similarly, the glycidol density increased with an increase in both reaction time and concentration. The maximum glycidol density was recorded at a reaction time of 107.36 min and concentration of 14.02 vol% after which there was no further increment achieved because of reaching full functionalization. Fig. 4c shows the 3D plot interaction between the temperature and reaction time at a constant concentration of 12.85 vol%, in which the glycidol density increases with a rise in temperature and reaction time. It can be observed that a maximum glycidol density was achieved when the temperature and reaction time is 77.46 °C and 114.14 min, respectively.

3.4. Experimental validation of glycidol density

The predicted value of glycidol density from the numerical optimization (model) was validated under a chosen optimum parameter of 11.8 vol%, 78.9 °C and 109.4 min for glycidol concentration, temperature, and reaction time, respectively in triplicate runs. It is worth mentioning that the desirability of the response for the selected parameters is 1, as such the validation experiment performed was found to be 4.98 mmol·g^{-1}. This value agrees well with the 4.97 mmol·g^{-1} glycidol density predicted with negligible deviation. Thus, this confirms a successful optimization of the glycidol density in the fibrous chela-

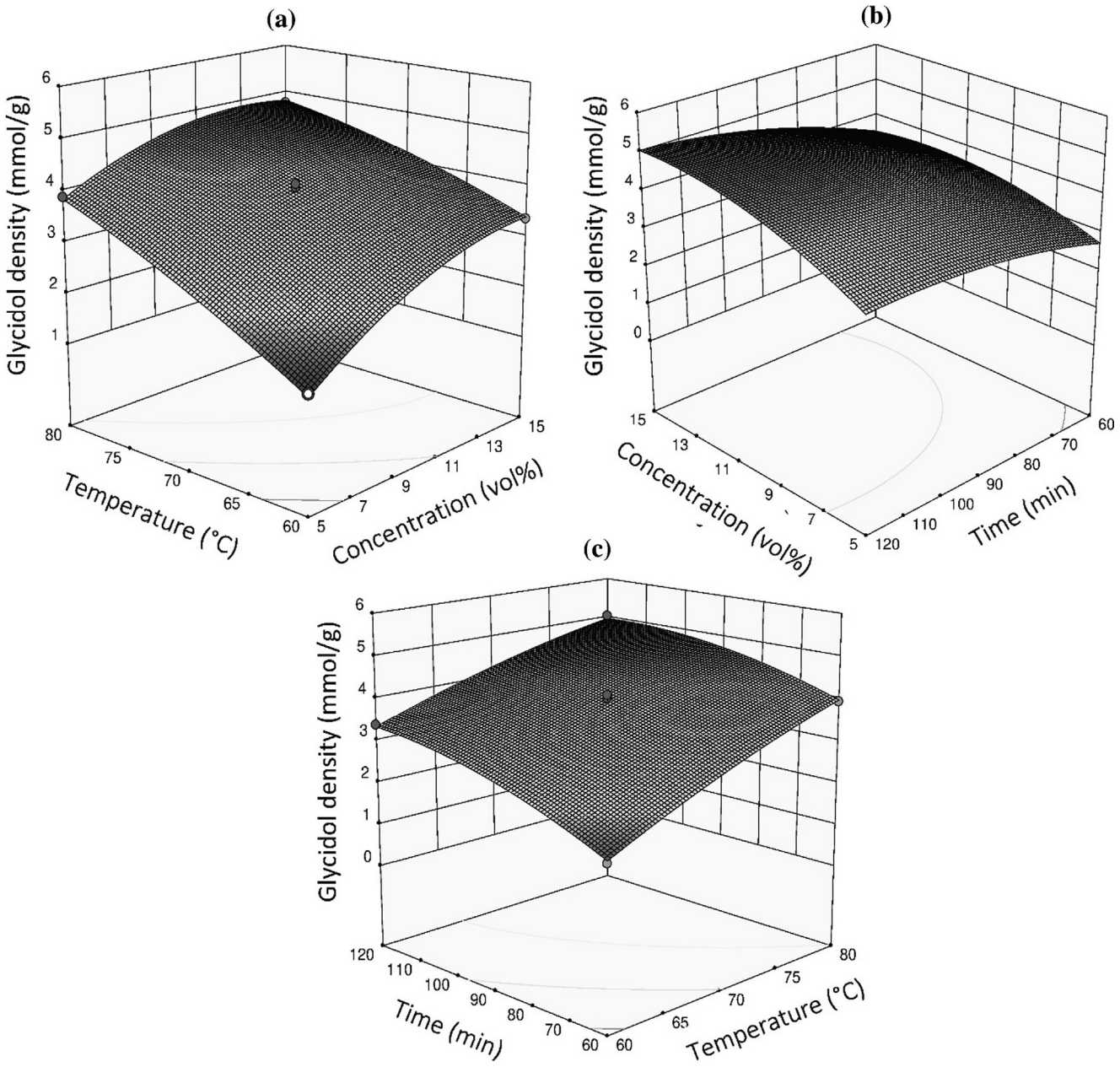

Fig. 4 Response surface plots for the effects of: (a) temperature vs. glycidol concentration, (b) reaction time vs. glycidol concentration (c) reaction time vs. temperature on the glycidol density in the chelator.

tor using BBD despite the use of three levels for the independent parameters' values in this study.

3.5. Properties of PE/PP-g-PVAm-G

The diffraction pattern of the PE/PP-*g*-PVAm-G chelator is shown in Fig. 5a. Five major crystalline peaks from the PE and PP substrate were observed to agree with previous studies (Afolabi et al., 2021a; Furukawa et al., 2006). This indicates that the chelator maintained its structural integrity required for the boron adsorption. The infra-red spectrum of the PE/PP-*g*-PVAm-G is presented in Fig. 5b. The band at 1032 cm^{-1} depicts the C—O stretching vibration of glycidol epoxy ring-opened linkage while the peak at 1244 cm^{-1} can be ascribed to amine's C—N stretching vibration. The peaks located at 2849 and 2916 cm^{-1} are associated with CH_2 antisymmetric and symmetric stretching of the PE/PP skeletal structure (Hayashi et al., 2018). The very broad and strong peak around 3323 cm^{-1} shows the presence of the O—H group for chelation in the material. These characteristics peaks are associated with chelating chelator for boron (Hoshina et al., 2021). Results of chemical changes resulting from grafting and hydrolysis were discussed in our previous publication (Afolabi et al., 2021a). The PE/PP-*g*-PVAm-G chelator's thermal stability is revealed by TGA. Fig. 5c depicts three stages of weight loss. The first weight loss in the temperature range of 32−140 °C is corresponding to the dehydration of the bound water molecules caused by the imparted hydrophilic character

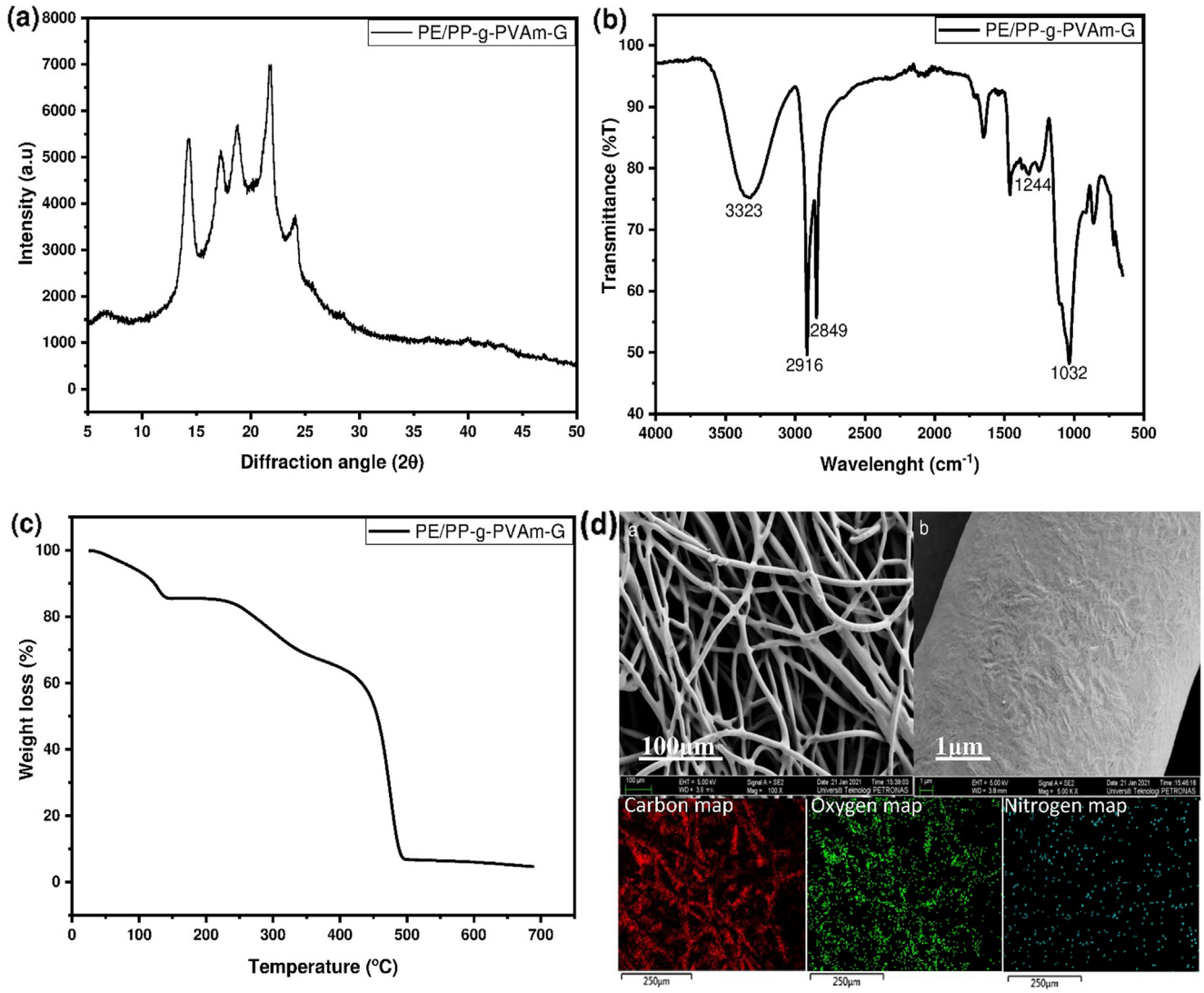

Fig. 5 (a) XRD pattern, (b) FTIR spectrum, (c) TGA thermogram and (d) FESEM-EDX mapping of PE/PP-*g*-PVAm-G.

resulting from incorporation of glycidol moiety. The second weight loss was at approximately 220−385 °C which can be ascribed to the PVAm grafts depolymerization. The third weight loss (385−480 °C) denotes a typical PE/PP substrate thermal decomposition transition (Xu et al., 2019). The FESEM image (Fig. 5d) corresponds to the structure of the PE/PP-*g*-PVAm-G with no apparent damage in the PE/PP non-woven fibrous sheet. The EDX mapping of PE/PP-*g*-PVAm-G results indicates that the fibrous chelator mainly contains C (76.9%), O (18.3%) and N (4.8%) elements. The rich distribution of O indicates a random functionalization and excellent dispersion of functional groups throughout the polymeric structure, thereby making it suitable for the adsorption of boron.

3.6. Exploring the factors influencing the experiment

3.6.1. Effect of pH

The distribution and quantity of each boron anion in the aqueous solution varies at different pH levels, likewise the forms at which they exist is complex. As a result, investigating boron-adsorbent complexation in various acid-base conditions is crucial. The influence of different pH solution ranges on the adsorption capacity of boron was investigated to determine the optimum pH value. The adsorption capacity of the chelator was found to initially increase from pH 2 until pH 7 beyond which it decreases as depicted from Fig. 6 illustrating the variation of adsorption capacity with pH of the treated solution. The increase in adsorption capacity with the increase in pH value can be attributed to the fact that fewer protons become available in the solution to compete with the boron ion for binding sites (glycidol) on the adsorbent surface as the pH increases (Oladipo and Gazi, 2016). At neutral pH, the adsorption capacity reaches its maximum value (21.4 $mg{\cdot}g^{-1}$) in which formation of bis-chelate ester complex is predominant. Further increase in pH values (pH great than 7) leads to a decrease in adsorption capacity due to competition between borate ions and the growing amount of hydroxyl groups in the solution. This behaviour can be explained by the fact that boric acid, $B(OH)_3$ is an extremely weak, monobasic acid (pKa = 9.23) that acts as a Lewis acid by accepting

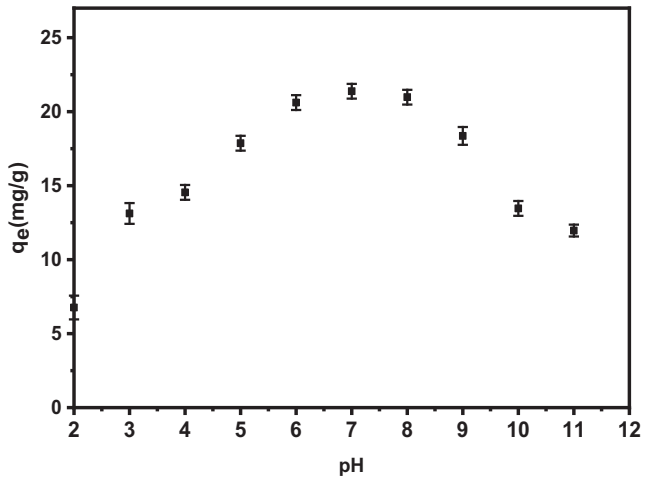

Fig. 6 Adsorption of boron by PE/PP-*g*-PVAm-G chelator as a function of pH.

hydroxyl groups in water to form $B(OH)_4^-$ species, rather than donating proton (Sanfeliu et al., 2012). Similar result was reported for adsorption of boron by boron-selective adsorbent with low-cost materials (Sanfeliu et al., 2012), and N-methylglucamine-type cellulose derivatives (Inukai et al., 2004). A comparison of the chelator in this study with different boron-selective adsorbents and commercial resins performance reported in literature are summarized in Table 6.

3.6.2. Adsorption equilibrium isotherms

Adsorption isotherm relates the quantity of adsorbate adsorbed onto the fibrous chelator to the quantity of adsorbate remaining in the solution once the adsorption process has reached equilibrium. The isotherm parameter values provide information about the chelator surface characteristic, as well as its affinity for the adsorbate, and are crucial for optimizing the chelator usage (Asare et al., 2021). Here, the adsorption isotherms examination is to demonstrate how the PE/PP-*g*-PVAm-G and the boron adsorbate are behaving when in contact with the solution. The fitting of adsorption isotherm data to various adsorption isotherm models is a critical step in determining the most appropriate adsorption isotherm model for design purposes. The amount of boron adsorbed onto PE/PP-*g*-PVAm-G was studied using six different adsorption isotherms including two parameters (Langmuir, Freundlich, and Temkin) and three parameters (Redlich-Peterson, Toth, and Sips) equations. Although linear isotherms have been utilized to describe adsorption systems in many studies, however, non-linear isotherms were used in this work for more accuracy. The adsorption isotherms were established based on certain assumptions. As a result, linearizing them would undermine the assumptions that influence their development and could lead to an erroneous solution. The non-linear form of the isotherms, despite its complexity, gives a remarkable and precise mathematical approach to compute the isotherm parameters. Hence, to prevent inaccuracy caused by linearization, the parameters of the various isotherms in this study were obtained with the non-linear technique.

The Langmuir isotherm model is representing the monolayer coverage of boron on the chelator surface at a constant temperature. It hints towards the homogeneity of the surface and assumes that the application of intermolecular forces by the chemical surface of unsaturated atoms does not extend furthermore than the adsorbed molecule diameter (Jin et al., 2019). This model also assumes that all adsorption sites have the same energy properties, and that adsorption takes place on a structurally homogeneous surface. The Langmuir equation has the following expression:

$$q_e = \frac{q_m K_L C_e}{1 + K_L C_e} \tag{5}$$

$$R_L = 1/(1 + K_L C_0) \tag{6}$$

where C_e and C_o are the liquid phase equilibrium concentration and initial concentration of boron. The equilibrium adsorption capacity is represented byq_e ($mg{\cdot}g^{-1}$), while the maximum amount of adsorbed boron per unit weight of the chelator is denoted by q_m ($mg{\cdot}g^{-1}$). The K_L ($L{\cdot}mg^{-1}$) is related to the Langmuir equilibrium constant with binding sites affinity indicating adsorption reaction bond energy between boron and chelator (Chen et al., 2019). The separation factor of Langmuir (R_L) indicates whether the adsorption is: favorable when R_L value is between 0 and 1, unfavorable when > 1; Irreversible when = 0 and linear when = 1.

The Freundlich adsorption isotherm model portrays the heterogeneity of the surface and the adsorbed molecule's multilayer adsorption. Therefore, it is generally used for heterogeneous systems, and the amount of adsorbed molecule is the aggregation of all the adsorption sites (each having bond

Table 6 Comparison of adsorption properties of the PE/PP-*g*-PVAm-G chelator in this study with previous studies for adsorbents containing vicinal diols.

Adsorbents material	Morphology	Ligands	T_e (min)	q_e ($mg{\cdot}g^{-1}$)	pH	References
Nylon-6 based adsorbent	Fibrous	NMDG	120	12.4	7	(Ikeda et al., 2011)
Terpolymer-based	Bead	Glycidol	30	17.3	6.5	(Gazi & Bicak, 2007)
Cellulose	Fibrous	NMDG	> 60	12.1	8.7	(Inukai et al., 2004)
Diaion CRB −03	Granules	NMDG	> 60	11.6	7	(Ting et al., 2016)
Chitosan	Bead	NMDG	400	20.4	7	(Wu et al., 2019)
Terpolymer-based	Bead	Glycidol	80	32.4	6.6	(Senkal & Bicak, 2003)
Nylon-6 based adsorbent	Fibrous	NMDG	30	13.8	7	(Ting et al., 2016)
Polyacrylonitrile	Nanofibrous	NMDG	100	5.5	6–7	(J. Wang et al. (2014b))
PP/PE based adsorbent	Fibrous	Glycidol	60	21.4	7	This study

T_e = Equilibrium time.

energy) (Luo et al., 2020b). The equation of Freundlich isotherm can be expressed in Eq. (7).

$$q_e = K_F C_e^{1/n} \tag{7}$$

where C_e (mgL^{-1}) represents the liquid phase equilibrium concentration and q_e ($mg{\cdot}g^{-1}$) is the adsorption capacity of boron at equilibrium, while K_F ($mg{\cdot}g^{-1}$)($L{\cdot}mg^{-1}$)$^{1/n}$ and 1/n represent the Freundlich constant as well as heterogeneity factor which indicates the intensity of adsorption, respectively.

The Temkin isotherm is derived on the assumption that the decrease in adsorption heat is linear rather than logarithmic and that the adsorption process is characterized by a uniform distribution of binding energies at the chelator surface. The non-linear equation of Temkin isotherm can be represented by:

$$q_e = \frac{RT}{b_T} In(A_T C_e) \tag{8}$$

where b_T and A_T are Temkin isotherm constants, RT/b_T is a constant related to the heat of adsorption. The absolute temperature and the universal gas constant (8.314 J mol^{-1} K^{-1}) are respectively denoted by T and R.

The Sips isotherm eliminates the limiting deficiencies associated with both Langmuir and Freundlich isotherms by combining them into a single equation (Asare et al., 2021). The Sips isotherm is expressed as:

$$q_e = \frac{q_s K_s C_e^{1/ns}}{1 + K_s C_e^{1/ns}} \tag{9}$$

where q_s ($mg{\cdot}g^{-1}$) is the Sips isotherm maximum adsorption capacity, while Ks (Lg^{-1}) is the Sips constant, and 1/ns is the Sips exponent. If 1/ns = 1, it denotes the process takes on a homogenous surface.

The Toth isotherm is a three-parameter isotherm that can be used for describing the adsorption behavior on a heterogeneous surface. The isotherm can describe how heterogeneous surface adsorption at low and high concentration boundaries of a particular adsorbate behaves. The Toth isotherm is written as follows:

$$q_e = \frac{q_t K_t C_e}{\left[1 + (K_t C_e)^t\right]^{1/t}} \tag{10}$$

where q_t ($mg{\cdot}g^{-1}$) represents the Toth maximal adsorption capacity, while K_t is the Toth isotherm constant, and the Toth exponent is 1/t. The isotherm simplifies to the Langmuir isotherm equation as t approaches unity (Asare et al., 2021).

Redlich-Peterson isotherm can be referred to as hybrid isotherm which features both Langmuir and Freundlich isotherms, with the existence of three parameters in the empirical equation (Foo and Hameed, 2010). Thus, due to its versatility, this model is applied for both homogenous and heterogeneous systems. The Redlich-Peterson isotherm can be expressed using Eq. (11).

$$q_e = \frac{K_R C_e}{1 + A_R C_e^g} \tag{11}$$

where C_e (mg/L) is the concentration at equilibrium in the liquid phase, and q_e ($mg{\cdot}g^{-1}$) is the adsorption capacity of boron at equilibrium, while A_R (mg^{-1}) and K_R (Lg^{-1}) are Redlich-Peterson adsorption isotherm constants. The isotherm exponent (g) values are ranging between 0 and 1. Different studies have proven Redlich-Peterson isotherm to be more accurate when compared with Langmuir and Freundlich isotherms due to the three unknown parameters involved in it and thus, both isotherms' derivations can be achieved from Eq. (11) (Foo and Hameed, 2010).

Fig. 7 represents the boron adsorption equilibrium isotherms for the PE/PP-*g*-PVAm-G chelator. The values of various constants and fitting data including the correlation coefficient R^2, and χ^2 are also listed in Table 7. According to the estimated data from the various models of the two-parameter isotherms, the Langmuir correlation coefficient R^2 is 0.9799, which is greater than the values for the other two isotherms. Moreover, it shows the least χ^2 (0.0092) value. This data suggests that monolayer adsorption occurred on a homogeneous surface during the adsorption process. The monolayer saturation capacity (q_m) for boron on PE/PP-*g*-PVAm-G was estimated as 25.7 $mg{\cdot}g^{-1}$ while the R_L values estimated were found to fall between 0 and 1 which gives an indication that the adsorption of boron is favorable (Kipçak and Özdemir, 2012; Oladipo and Gazi, 2016). Consequently, in the Freundlich isotherm model, the 1/n value obtained is below one. This suggests that the adsorption process followed a favorable

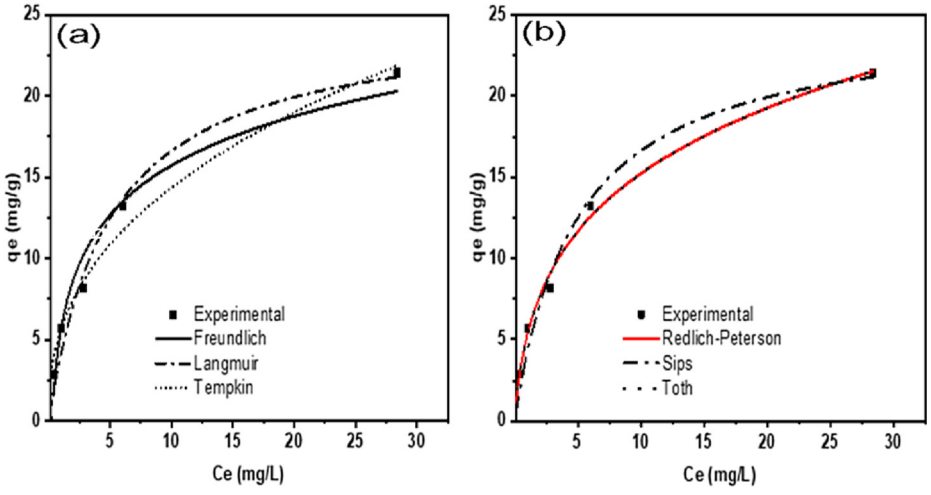

Fig. 7 Plots of: (a) two-parameter and (b) three-parameter isotherms of boron adsorption by PE/PP-*g*-PVAm-G.

Table 7 Two-parameter isotherms for boron adsorption onto PE/PP-*g*-PVAm-G.

Langmuir	Freundlich	Temkin
K_L = 0.203	K_F = 5.18	A_T = 3.68
q_m = 25.7	1/n = 0.403	RT/b_T = 11
R^2 = 0.9799	R^2 = 0.9528	R^2 = 0.9659
χ^2 = 0.0092	χ^2 = 0.191	χ^2 = 2.423

normal Langmuir isotherm as indicated by the R_L values. The adsorption process is not represented by Temkin isotherm due to its correlation coefficient value, however, the heat of adsorption RT/b_T was estimated as 11 kJ mol^{-1}. The typical range of bonding energy for ion-exchange mechanisms has been reported in the range of 8–16 kJ mol^{-1} (Baker, 2009; Wei et al., 2011).

From Table 8, the correlation coefficient R^2 of the three-parameter isotherms is higher than all the two-parameter isotherms. This is suggesting the applicability of three-parameter isotherm models to represent the adsorption equilibrium of boron by PE/PP-*g*-PVAm-G chelator. The correlation coefficients in Redlich-Peterson, Toth and Sips are 0.9953, 0.9951 and 0.9858, respectively. The Redlich-Peterson and Toth adsorption model showed the highest R^2 value and leads to the best regression coefficients. Similar result was observed by Benzaoui et al. (2018). More so, both the Redlich-Peterson and Toth isotherm constant values i.e., g and t are not far from unity, indicating that it is approaching the Langmuir isotherm but not the Freundlich isotherm. Thus, Langmuir is a special case of Redlich-Peterson when the constant g approaches unity (Ayawei et al., 2017; Ding et al., 2017). The value of the Sips isotherm constant (1/ns) also approaches unity too, suggesting that boron uptake by PE/PP-*g*-PVAm-G occurs on a homogenous surface. This finding is consistent with the two-parameter isotherm analysis. Comparable results were reported for nanofibrous chelator containing NMDG counterpart for boron removal (Nallappan et al., 2019).

3.6.3. Adsorption kinetics

The adsorption kinetics show how the adsorption process changes over time. Thus, the latter is a critical variable that must be considered. The pseudo-first-order, pseudo-second-order, and intraparticle diffusion models were considered for the determination of the suitable model as well as for the explanation of the experimental data mechanism. The pseudo-first-order adsorption model theorized that the rate is proportional to the number of the unoccupied adsorption sites and is expressed as:

Table 8 Three-parameter isotherms for boron adsorption onto PE/PP-*g*-PVAm-G.

Redlich-Peterson	Toth	Sips
K_R = 11.57	K_t = 1.29	Ks = 5.52
A_R = 1.21	q_t = 6.63	qs = 24.85
g = 0.74	t = 0.97	1/ns = 1.103
R^2 = 0.9953	R^2 = 0.9951	R^2 = 0.9858
χ^2 = 0.0003	χ^2 = 0.477	χ^2 = 1.429

$$q_t = q_e(1 - e^{-k_1 t}) \tag{12}$$

where q_e ($mg{\cdot}g^{-1}$) is the adsorption capacity of boron at equilibrium and q_t is the adsorption capacity of boron at any given time t (min). The k_1 (min^{-1}) represents the equilibrium rate constant for the pseudo-first-order model.

The pseudo-second-order rate expression is used to explain the chemisorption that involves valence forces through the exchange or sharing of electron as ion exchange and covalent forces between the adsorbent and adsorbate. The second-order rate expression is given below:

$$q_t = \frac{q_e^2 k_2 t}{1 + k_2 q_e t} \tag{13}$$

where q_e ($mg{\cdot}g^{-1}$) is the boron adsorption capacity at equilibrium and q_t is the adsorption capacity of boron at any given time t (min). k_2 (min^{-1}) represents the pseudo-second-order equilibrium rate constant.

Fig. 8 shows the kinetic models with the impact of contact time on the removal of boron by PE/PP-*g*-PVAm-G at different concentrations and contact time. During the process of adsorption, the chelator was able to adsorb 70–85% of the saturated adsorption capacity within 30 min, and the chelator reaches the saturated adsorption capacity within 60 min because PE/PP-*g*-PVAm-G is rich in polyols. Henceforth, a substantial amount of boron diffused to the surface of the chelator at the start of the adsorption reaction, and the polyols and boron were continually complexed. As boron continuously occupies the adsorption sites, the adsorption rate is reduced until all of the adsorption sites are filled up, and the amount adsorbed tended to become saturated and constant (Luo et al., 2020b). Table 9 shows the data for pseudo-first-order rate constants k_1, pseudo-second-order rate constants k_2, calculated equilibrium adsorption capacity $q_{e(cal)}$, R^2, and χ^2 for better understanding of the adsorption mechanism such as mass transfer and chemical reaction. The kinetics fitting results for the models indicate that the process does not follow pseudo-first-order kinetics. The pseudo-second-order kinetic best fit the experimental data as it provides the highest R^2, and lowest χ^2 values at different initial concentrations than the pseudo-first-order kinetic. This is because the pseudo-

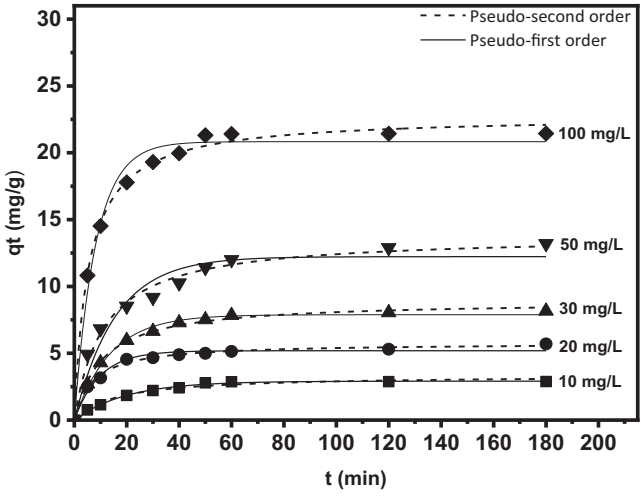

Fig. 8 The Kinetic models plots for boron adsorption by the PE/PP-*g*-PVAm-G.

Table 9 The adsorption kinetic parameters for boron adsorption by PE/PP-*g*-PVAm-G.

Kinetic models	Parameters	10 mg/L	20 mg/L	30 mg/L	50 mg/L	100 mg/L
Pseudo-first order	$q_{e,(calc)}$ ($mg{\cdot}g^{-1}$)	2.51	5.18	7.38	11.23	20.03
	k_1 (min^{-1})	0.050	0.103	0.073	0.064	0.12
	R^2	0.9811	0.9776	0.9936	0.9488	0.9872
	χ^2	0.022	0.077	0.053	0.972	0.759
Pseudo-second order	$q_{e,(calc)}$ ($mg{\cdot}g^{-1}$)	3.05	5.77	8.90	13.82	22.76
	k_2 ($g{\cdot}mg^{-1}{\cdot}min^{-1}$)	0.019	0.025	0.011	0.064	0.0081
	R^2	0.9945	0.9932	0.9959	0.9872	0.9964
	χ^2	0.007	0.0231	0.0337	0.243	0.190
Intraparticle diffusion	k_p ($mg{\cdot}g^{-1}{\cdot}min^{1/2}$)	0.190	0.26	0.399	0.659	0.732
	C ($mg{\cdot}g^{-1}$)	0.94	2.83	3.89	5.33	13.94
	R^2	0.7066	0.7477	0.7298	0.796	0.6607
	χ^2	0.407	0.509	0.823	1.133	1.80

second-order kinetic q_e values calculated corroborate more with the experimental results. Thus, the consistency of the ion exchange adsorption process with pseudo-second-order kinetic model further shows that the complexation between $B(OH)_3$ and the polyol groups from the chelator is controlled by chemical interaction (Lyu et al., 2017; Uba et al., 2020).

3.6.4. Mechanism of boron removal by PE/PP-g-PVAm-G

The mechanism involved in the boron removal by PE/PP-*g*-PVAm-G was evaluated with Eq. (14). The intraparticle diffusion model was adopted in this context. It is based on the theory that the fraction of boron removed depends on the chelating diffusivity of PE/PP-*g*-PVAm-G and the radius of boron. The intra-particle diffusion model expression is given as:

$$q_t = k_p t^{1/2} + C \tag{14}$$

where k_p ($mg^{-1}{\cdot}g^{-1}{\cdot}min^{-2}$) is determined from the plot of q_t versus $t^{1/2}$ as the intra-particle diffusion rate constant and C ($mg{\cdot}g_{ad}^{-1}$) represents the boundary layer thickness and intercept. It is worth noting that the plot of q_t versus $t^{1/2}$ provides a straight line through the origin for an adsorption process where intraparticle diffusion is the rate controlling step (Yao and Chen, 2017). However, the plot in Fig. 9 does not generate a straight line passing through the origin. This implies the presence of boundary layer, suggesting that intraparticle diffusion was not the sole mechanism controlling the removal process but other mechanisms were involved which has a chemisorption nature (Asare et al., 2021; Nallappan et al., 2019). Two major stages could be seen in the plot from Fig. 9. The first stage is faster and depicts the intraparticle diffusion where boron got transported from the surface of PE/PP-*g*-PVAm-G to its interior pores. The second stage is relatively slower and can be attributed to the attachment of boron to the active adsorption sites on the interior surface of PE/PP-*g*-PVAm-G through chemisorption. The external surface adsorption was less apparent, and this could be attributed to the fast boron diffusion onto the external surface of PE/PP-*g*-PVAm-G. This suggests that the first stage of diffusion is very fast and almost very instantaneous for this polymeric fibrous chelator when compared with granular adsorbents. This can be ascribed to the chelator's decreased in size and subsequent increase in the surface area coupled with the rise in the number of functional groups caused by higher glycidol density leading to a larger number of sorption sites which fastened the adsorption rate. The intercept is an indicator of the boundary layer thickness, suggesting a greater boundary layer effect on the adsorption process at high initial boron ion concentrations. This result is consistent with previous study on nanofibrous adsorbents for boron removal (Ting et al., 2016).

3.6.5. Adsorption thermodynamics studies

The evaluation of thermodynamic parameters such as enthalpy (ΔH^o), Gibbs free energy (ΔG^o), and entropy (ΔS^o) changes was carried out to comprehend the nature and feasibility of the adsorption process. This can be achieved from the changes in temperature (T) and thermodynamic equilibrium constant (K_C). They were calculated from the following equations:

$$K_C = \frac{C_{Ad}}{C_e} \tag{15}$$

where C_{Ad} and C_e are respectively representing the equilibrium concentrations of boron on PE/PP-g-PVAm-G and in the solution (mgL^{-1}). The Gibbs free energy change ($\Delta G°$) gives an indication of the adsorption process degree of spontaneity, its high negative value denotes a more energetically favorable

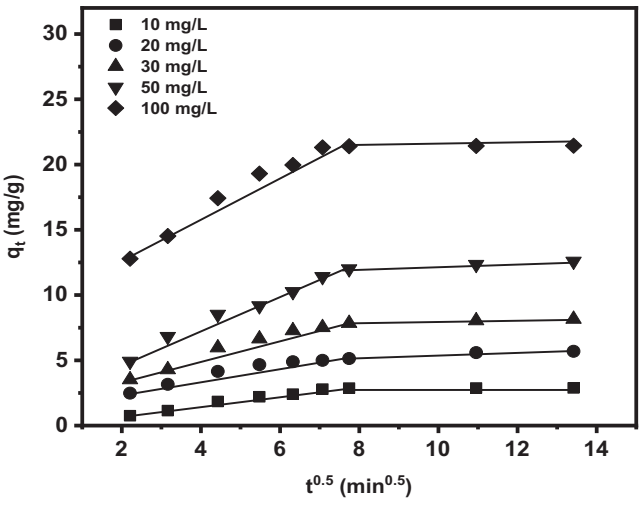

Fig. 9 The intra-particle diffusion plots of boron adsorption by the PE/PP-*g*-PVAm-G.

adsorption (Mananghaya et al., 2016). Thus, the ΔG^{o} for the adsorption process can be estimated from the equation:

$$\Delta G^{\circ} = -RTInK_C \quad (16)$$

where T and R are the absolute temperature in Kelvin and gas constant (8.314 $Jmol^{-1}K^{-1}$) respectively. Meanwhile, ΔH^{o} and ΔS^{o} values are obtained using Van't Hoff equation below:

$$InK_C = -\frac{\Delta G}{RT} = -\frac{\Delta H}{RT} + \frac{\Delta S}{R} \quad (17)$$

From the intercept and slope of the plot from $\ln K_C$ versus 1/T, ΔH^{o} and ΔS^{o} values were calculated and summarized in Table 10. The negative values of ΔG° indicate that the boron adsorption on PE/PP-*g*-PVAm-G is spontaneous, and the free energy value swings. Not only that but also ΔG° became more negative as temperature increased, implying a greater driving force and hence a bigger adsorption capacity at higher temperatures which further demonstrates that boron adsorption is spontaneous and thermodynamically favorable (Lyu et al., 2017). The positive values of ΔH^{o} (5.541 kJ mol^{-1}) confirm the endothermic nature of adsorption, while the positive value of ΔS^{o} (25.829 J mol^{-1} K^{-1}) suggests an increased degree of randomness at the solid–liquid interface during the process of boron adsorption onto PE/PP-*g*-PVAm-G. Similar observation was reported for boron removal from solution (Zijie Wang et al., 2021).

3.6.6. Boron adsorption in the presence of foreign ions

The presence of a large number of inorganic salts which are ionizable into various ions in aqueous solutions can reduce the chelator's adsorption capacity in surface water, industrial wastewater, and subsurface water sources. As a result, studying the selectivity properties of PE/PP-*g*-PVAm-G towards anions and cations in solutions is important. The adsorption selectivity study was conducted in the presence of foreign ions such as Na^{+}, Ca^{2+}, Cl^{-} and SO_4^{2-}. The sources of the various ions used in this study were NaCl, $CaCl_2$, KCl, and Na_2SO_4. The experiments revealed that, in the presence of boric acid, these foreign ions are also absorbed. The highest loading is observed for Ca^{2+} ions (1.67 $mg{\cdot}g^{-1}$) as shown in Fig. 10. The foreign ion adsorption observed could be due to the precipitation of their hydroxides and the weak basicity of the tertiary amino group from the polymeric substrate (Gazi and Shahmohammadi, 2012). Fortunately, adsorption of those coexisting ions does not show a significant decrease in the boron loading capacity of PE/PP-*g*-PVAm-G. This may be due to the coordination capability of the polyol of the chelator. Not only that but may also be due to the influence of the inorganic salt ions occupying some of PE/PP-*g*-PVAm-G active sites, resulting in a modest reduction in boron adsorption capacity. Therefore, the chelator can be said to have good boron selectivity as well as anti-interference properties.

Table 10 Thermodynamic parameters for boron adsorption on PE/PP-*g*-PVAm-G chelator.

Temperature (°C)	ΔG° (kJ mol^{-1})	ΔH^{o} (kJ mol^{-1})	ΔS^{o} (J mol^{-1} K^{-1})
293	−2.005		
303	−2.331	5.541	25.829
313	−2.518		

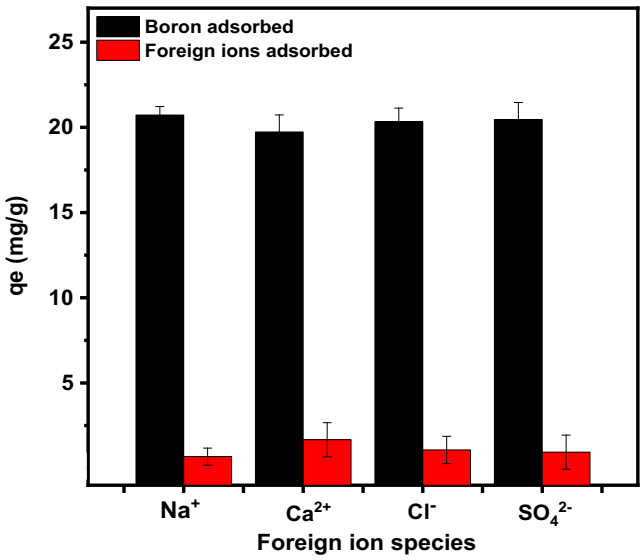

Fig. 10 Adsorption capacities of the PE/PP-*g*-PVAm-G for boron and coexisting ions in simulated water.

3.7. Re-usability study

The regeneration cycle result for the elution process is presented in Fig. 11. The result showed a trivial increase in capacity loss with a decrease in adsorptive efficiency after five adsorption/desorption cycles as evidenced by Fig. 11. This observation can be attributed to the fact that there is a decrease in active sites of PE/PP-*g*-PVAm-G. The decline in efficiency is $<3\%$ which indicates that the PE/PP-*g*-PVAm-G has a high recyclability and nearly maintains a constant regeneration efficiency after 5 cycles. The result implied that PE/PP-*g*-PVAm-G could be successfully regenerated as an

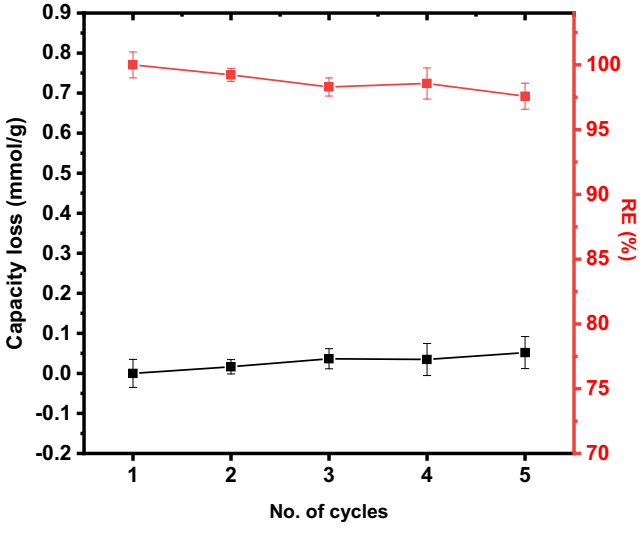

Fig. 11 Re-usability of PE/PP-*g*-PVAm-G for boron adsorption.

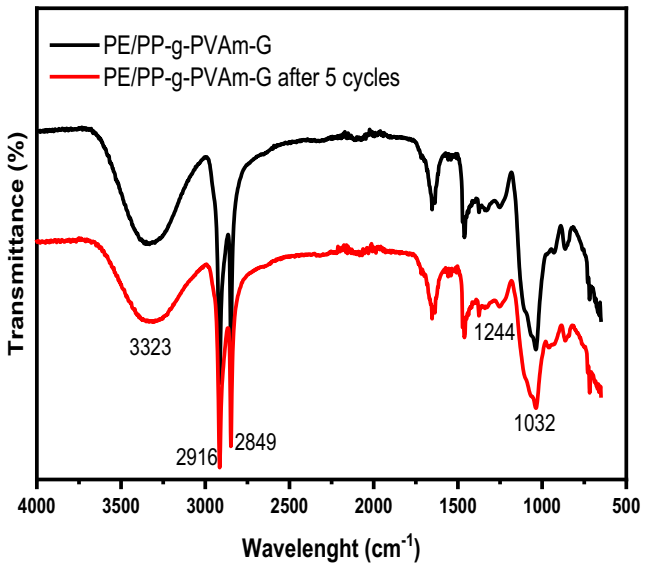

Fig. 12 IR of PE/PP-*g*-PVAm-G before and after 5 cycles.

effective adsorbing material for removing boron from contaminated solutions.

After the PE/PP-*g*-PVAm-G chelator is subjected to 5 cycles of adsorption–desorption, the changes in mass before and after adsorption was observed to be negligible. The infrared spectroscopy comparison of PE/PP-*g*-PVAm-G before and after the 5 cycles is displayed (Fig. 12). The results reveal that the PE/PP-*g*-PVAm-G functional groups remained unaltered after the 5 cycles of adsorption–desorption. This gives an indication that the fibrous chelator has a promising regeneration stability. To make the process green, the recovery of boron and the acid used to strip it should be considered to reach the pure water discharge. The recovered acid and boron can be further used.

4. Conclusions

PE/PP-*g*-PVAm-G fibrous chelator containing *cis*-diol groups was successfully prepared by RIGC of NVF onto PP/PE nonwoven sheet followed by conversion of polyamide grafts to polyamine and subsequent chemical treatments with glycidol and tested for boron adsorption from aqueous solution. The reaction variables were optimized using RSM to maximize the glycidol density on the chelator. A maximum glycidol density yield of ~5.0 mmol·g^{-1} was obtained at 11.8 vol%, 78.9 °C, and 109.4 min for glycidol concentration, temperature, and time, respectively. The FT-IR, SEM, EDX, DSC, and TGA analysis of the adsorbents revealed convincing proof of chemical treatment and covalent immobilization of the glycidol groups onto PVAm. The boron adsorption data was best represented by the Langmuir from the two-parameter isotherm, suggesting that the adsorption process occurs on a homogenous surface by monolayer adsorption with a maximum adsorption capacity of 25.7 mg·g^{-1}. The three-parameter isotherm model correlation coefficient was higher than all the two-parameter isotherms. Thus, suggesting their applicability and gives an indication that the Langmuir is a special case of Redlich-Peterson. The adsorption process kinetics revealed that the uptake of boron followed a second-order kinetic path. This implies that the process occurred by chemical attachment of the boron to the polyol groups of PE/PP-*g*-PVAm-G as a chelator. The spontaneous removal process was found to be endothermic with ΔH^o of 5.541 kJ mol^{-1} and random in nature with ΔS^o of 25.829 J mol^{-1} K^{-1}. Na^+, Ca^{2+}, Cl^- and SO_4^{2-} ions had little effect on the PE/PP-*g*-PVAm-G adsorption capacity of boron. The fibrous chelator has a good recyclability and virtually maintained a steady regeneration efficiency after 5 cycles. The results demonstrated that PE/PP-*g*-PVAm-G can be used as an alternative adsorbent in terms of adsorption capacity, selectivity, and re-usability for removing boron from aqueous solutions.

Acknowledgments

The authors are appreciative of the financial support provided by Universiti Teknologi Petronas through the grant of Y-UTP with the cost center 015LC0-065 and 015LC0-310. The Malaysian Nuclear Agency's invaluable technical assistance during the radiation grafting processes is well appreciated.

Declaration of Competing Interest

The authors declare that they have no known competing financial interests or personal relationships that could have appeared to influence the work reported in this paper.

Data availability

The raw/processed data required to reproduce these findings cannot be shared at this time as the data also forms part of an ongoing study.

References

Afolabi, H.K., Nasef, M.M., Nordin, N.A.H.M., Ting, T.M., Harun, N.Y., Abbasi, A., 2021a. Facile preparation of fibrous glycidol-containing adsorbent for boron removal from solutions by radiation-induced grafting of poly(vinylamine) and functionalisation. Radiat. Phys. Chem. 188, 109596. https://doi.org/10.1016/j.radphyschem.2021.109596.

Afolabi, H.K., Nasef, M.M., Hadi Sapiaa, N.A.M., Harun, N.Y., Ting, T.M., Hui, T.T., 2021b. Highly boron-selective adsorbent by radiation induced grafting of N-vinylformamide on polyethylene/polypropylene sheet followed by hydrolysis and glycidol treatment. Radiat. Phys. Chem. 182, 109362. https://doi.org/10.1016/j.radphyschem.2021.109362.

Asare, E.A., Dartey, E., Sarpong, K., Effah-Yeboah, E., Amissah-Reynolds, P.K., Tagoe, S., Balali, G.I., 2021. Adsorption isotherm, kinetic and thermodynamic modelling of bacillus subtilis ATCC13952 mediated adsorption of arsenic in groundwaters of selected gold mining communities in the wassa west municipality of the western region of Ghana. Am. J. Anal. Chem. 12, 121–161. https://doi.org/10.4236/ajac.2021.125010.

Ayawei, N., Ebelegi, A.N., Wankasi, D., 2017. Modelling and interpretation of adsorption isotherms. J. Chem. 2017, 1–11. https://doi.org/10.1155/2017/3039817.

Baker, H.M., 2009. A study of the binding strength and thermodynamic aspects of cadmium and lead ions with natural silicate minerals in aqueous solutions. Desalination 242 (1-3), 115–127. https://doi.org/10.1016/j.desal.2008.02.035.

Benzaoui, T., Selatnia, A., Djabali, D., 2018. Adsorption of copper (II) ions from aqueous solution using bottom ash of expired drugs incineration. Adsorpt. Sci. Technol. 36 (1-2), 114–129. https://doi.org/10.1177/0263617416685099.

Bezerra, M.A., Santelli, R.E., Oliveira, E.P., Villar, L.S., Escaleira, L. A., 2008. Response surface methodology (RSM) as a tool for optimization in analytical chemistry. Talanta 76 (5), 965–977. https://doi.org/10.1016/j.talanta.2008.05.019.

Chen, M., Dollar, O., Shafer-Peltier, K., Randtke, S., Waseem, S., Peltier, E., 2020. Boron removal by electrocoagulation: removal mechanism, adsorption models and factors influencing removal. Water Res. 170, 115362. https://doi.org/10.1016/j.watres.2019.115362.

Chen, Y., Lyu, J., Wang, Y., Chen, T., Tian, Y., Bai, P., Guo, X., 2019. Synthesis, characterization, adsorption, and isotopic separation studies of pyrocatechol-modified MCM-41 for efficient boron removal. Ind. Eng. Chem. Res. 58 (8), 3282–3292. https://doi.org/10.1021/acs.iecr.8b0474810.1021/acs.iecr.8b04748.s001.

Ding, W., Bai, S., Mu, H., Naren, G., 2017. Investigation of phosphate removal from aqueous solution by both coal gangues. Water Sci. Technol. 76, 785–792. https://doi.org/10.2166/wst.2017.241.

Dydo, P., Turek, M., 2013. Boron transport and removal using ion-exchange membranes : a critical review. Desalination 310, 2–8. https://doi.org/10.1016/j.desal.2012.08.024.

Ezechi, E.H., Isa, M.H., Rahman, S., Kutty, M., 2012. Boron in produced water: challenges and improvements : a comprehensive review. J. Appl. Sci. https://doi.org/10.3923/jas.2012.402.415.

Foo, K.Y., Hameed, B.H., 2010. Insights into the modeling of adsorption isotherm systems. Chem. Eng. J. 156 (1), 2–10. https://doi.org/10.1016/j.cej.2009.09.013.

Furukawa, T., Sato, H., Kita, Y., Matsukawa, K., Yamaguchi, H., Ochiai, S., Siesler, H.W., Ozaki, Y., 2006. Molecular structure, crystallinity and morphology of polyethylene/ polypropylene blends studied by Raman mapping, scanning electron microscopy, wide angle X-ray diffraction, and differential scanning calorimetry. Polym. J. 38 (11), 1127–1136. https://doi.org/10.1295/polymj.PJ2006056.

Gazi, M., Bicak, N., 2007. Selective boron extraction by polymer supported 2-hydroxylethylamino propylene glycol functions. React. Funct. Polym. 67 (10), 936–942. https://doi.org/10.1016/j.reactfunctpolym.2007.05.019.

Gazi, M., Shahmohammadi, S., 2012. Removal of trace boron from aqueous solution using iminobis-(propylene glycol) modified chitosan beads. React. Funct. Polym. 72 (10), 680–686. https://doi.org/10.1016/j.reactfunctpolym.2012.06.016.

Güler, E., Kaya, C., Kabay, N., 2015. Boron removal from seawater : State-of-the-art review. Desalination 356, 85–93. https://doi.org/10.1016/j.desal.2014.10.009.

Hayashi, N., Chen, J., Seko, N., 2018. Nitrogen-containing fabric adsorbents prepared by radiation grafting for removal of chromium from wastewater. Polymers (Basel) 10 (7), 744. https://doi.org/10.3390/polym10070744.

Herschy, R.W., 2012. Water quality for drinking: WHO guidelines. Encycl. Earth Sci. Ser. 876–883. https://doi.org/10.1007/978-1-4020-4410-6_184.

Hoshina, H., Chen, J., Amada, H., Seko, N., 2021. Chelating fabrics prepared by an organic solvent-free process for boron removal from water. Polymers 13 (7), 1163. https://doi.org/10.3390/polym13071163.

Ikeda, K., Umeno, D., Saito, K., Koide, F., Miyata, E., Sugo, T., 2011. Removal of boron using nylon-based chelating fibers. Ind. Eng. Chem. Res. 50 (9), 5727–5732. https://doi.org/10.1021/ie101968h.

Ince, A., Karagoz, B., Bicak, N., 2013. Solid tethered imino-bis-propanediol and quaternary amine functional copolymer brushes for rapid extraction of trace boron. DES 310, 60–66. https://doi.org/10.1016/j.desal.2012.06.017.

Inukai, Y., Tanaka, Y., Matsuda, T., Mihara, N., Yamada, K., Nambu, N., Itoh, O., Doi, T., Kaida, Y., Yasuda, S., 2004. Removal of boron(III) by N-methylglucamine-type cellulose derivatives with higher adsorption rate. Anal. Chim. Acta 511 (2), 261–265. https://doi.org/10.1016/j.aca.2004.01.054.

Jin, J., Du, X., Yu, J., Qin, S., He, M., Zhang, K., Yang, J., 2019. Synthesis of negatively charged polyol-functional PSF membranes with good hydrophilic and efficient boron removal properties. Polymers (Basel). 11, 780. https://doi.org/10.3390/polym11050780.

Kluczka, J., Korolewicz, T., Zołotajkin, M., Adamek, J., 2015. Boron removal from water and wastewater using new polystyrene-based resin grafted with glycidol. Water Resour. Ind. 11, 46–57.

Kabay, N., Bryjak, M., Schlosser, S., Kitis, M., Avlonitis, S., Matejka, Z., Al-Mutaz, I.M.Y., 2008. Boron method swot analysis. Desalination 223, 38–48.

Kamcev, J., Taylor, M.K., Shin, D.-M., Jarenwattananon, N.N., Colwell, K.A., Long, J.R., 2019. Functionalized porous aromatic frameworks as high- performance adsorbents for the rapid removal of boric acid from water. Adv. Mater. 31 (18), 1808027. https://doi.org/10.1002/adma.v31.1810.1002/adma.201808027.

Kipçak, I., Özdemir, M., 2012. Removal of boron from aqueous solution using calcined magnesite tailing. Chem. Eng. J. 189–190, 68–74. https://doi.org/10.1016/j.cej.2012.02.025.

Landi, M., Margaritopoulou, T., Papadakis, I.E., Araniti, F., 2019. Boron toxicity in higher plants: an update. Planta 250 (4), 1011–1032. https://doi.org/10.1007/s00425-019-03220-4.

Lin, J.-Y., Mahasti, N.N.N., Huang, Y.-H., 2021. Recent advances in adsorption and coagulation for boron removal from wastewater: a comprehensive review. J. Hazard. Mater. 407, 124401. https://doi.org/10.1016/j.jhazmat.2020.124401.

Luo, Q., He, L., Wang, X., Huang, H., Wang, X., Sang, S., Huang, X., 2020a. Science of the total environment cyclodextrin derivatives used for the separation of boron and the removal of organic pollutants. Sci. Total Environ. 749, 141487. https://doi.org/10.1016/j.scitotenv.2020.141487.

Luo, Q., Zeng, M., Wang, X., Huang, H., Wang, X., Liu, N., Huang, X., 2020b. Glycidol-functionalized macroporous polymer for boron removal from aqueous solution React. Funct. Polym. 150. https://doi.org/10.1016/j.reactfunctpolym.2020.104543.

Lyu, J., Zhang, N., Liu, H., Zeng, Z., Zhang, J., Bai, P., Guo, X., 2017. Adsorptive removal of boron by zeolitic imidazolate framework: kinetics, isotherms, thermodynamics, mechanism and recycling. Sep. Purif. Technol. 187, 67–75. https://doi.org/10.1016/j.seppur.2017.05.059.

Mananghaya, M., Yu, D., Santos, G.N., Rodulfo, E., 2016. Adsorption of mercury(II) chloride and carbon dioxide on graphene/calcium oxide (0 0 1). Korean J. Mater. Res. 26, 298–305. https://doi.org/10.3740/MRSK.2016.26.6.298.

Melo, L.L.A., Ide, A.H., Duarte, J.L.S., Zanta, C.L.P.S., Oliveira, L. M.T.M., Pimentel, W.R.O., Meili, L., 2020. Caffeine removal using Elaeis guineensis activated carbon: adsorption and RSM studies. Environ. Sci. Pollut. Res. 27 (21), 27048–27060. https://doi.org/10.1007/s11356-020-09053-z.

Meng, J., Cao, J., Xu, R., Wang, Z., Sun, R., 2016. Hyperbranched grafting enabling simultaneous enhancement of the boric acid uptake and the adsorption rate of a complexing membrane. J. Mater. Chem. 4 (30), 11656–11665. https://doi.org/10.1039/C6TA02348G.

Moawia, R.M., Nasef, M.M., Mohamed, N.H., Ripin, A., Zakeri, M., Hasimah, N., 2019. Biopolymer catalyst for biodiesel production by functionalisation of radiation grafted flax fibres with diethylamine under optimised conditions. Radiat. Phys. Chem. 164, 108375. https://doi.org/10.1016/j.radphyschem.2019.108375.

Najid, N., Kouzbour, S., Ruiz-García, A., Fellaou, S., Gourich, B., Stiriba, Y., 2021. Comparison analysis of different technologies for the removal of boron from seawater: a review. J. Environ. Chem. Eng. 9 (2), 105133. https://doi.org/10.1016/j.jece:2021.105133.

Nallappan, M.L., Nasef, M.M., Ting, T.M., 2019. Removal of boron from aqueous solutions using electrospun PVDF nanofibrous adsorbent modified by poly(glycidyl methacrylate)/ glucamine ligands. Desalin. Water Treat. 140, 163–171. https://doi.org/10.5004/dwt.2019.23361.

Nallappan, M.L., Nasef, M.M., Ting, T.M., Ahmad, A., 2018. An optimized covalent immobilization of glucamine on electrospun nanofibrous poly(vinylidene fluoride) sheets grafted with oxirane groups for higher boron adsorption. Fibers Polym. 19 (8), 1694–1705. https://doi.org/10.1007/s12221-018-8110-6.

Nasef, M.M., Nallappan, M.L, Ujang, Z., 2014. Polymer-based chelating adsorbents for the selective removal of boron from water and wastewater: a review. React. Funct. Polym. 85, 54–68. https://doi.org/10.1016/j.reactfunctpolym.2014.10.007.

Nesterov, D.V., Molochnikov, L.S., Kodess, M.I., Matochkina, E.G., Koryakova, O.V., Yatluk, Yu.G., Pestov, A.V., 2013. Synthesis of poly[N-(2,3-dihydroxypropyl)aminostyrene], a new sorbent for boron(III) ions. Russ. J. Appl. Chem. 86 (5), 777–781. https://doi.org/10.1134/S1070427213050273.

Oladipo, A.A., Gazi, M., 2016. Hydroxyl-enhanced magnetic chitosan microbeads for boron adsorption: parameter optimization and selectivity in saline water. React. Funct. Polym. 109, 23–32. https://doi.org/10.1016/j.reactfunctpolym.2016.09.005.

Recepoğlu, Y.K, Kabay, N., Yılmaz-İpek, İ., Arda, M., Yüksel, M., Yoshizuka, K., Nishihama, S., 2017. Deboronation of geothermal water using N-methyl-D-glucamine based chelating resins and a novel fiber adsorbent: batch and column studies. J. Chem. Technol. Biotechnol. 92 (7), 1540–1547. https://doi.org/10.1002/jctb.5234.

Recepoğlu, Y.K., Kabay, N., Ipek, I.Y., Arda, M., Yüksel, M., Yoshizuka, K., Nishihama, S., 2018. Packed bed column dynamic study for boron removal from geothermal brine by a chelating fiber and breakthrough curve analysis by using mathematical models. Desalination 437, 1–6. https://doi.org/10.1016/j.desal.2018.02.022.

Sanfeliu, C., Martínez-Máñez, R., Sancenón, F., Soto, J., Amorós, P., Azaïs, T., Marcos, M.D., 2018. 11B-MAS NMR approach to the boron adsorption mechanism on a glucose-functionalised mesoporous silica matrix. Microporous Mesoporous Mater. 266, 232–241. https://doi.org/10.1016/j.micromeso.2018.02.016.

Sanfeliu, C., Martínez-Máñez, R., Sancenón, F., Soto, J., Puchol, V., Amorós, P., Marcos, M.D., 2012. Low-cost materials for boron adsorption from water. J. Mater. Chem. 22, 25362–25372. https://doi.org/10.1039/c2jm32819d.

Senkal, B.F., Bicak, N., 2003. Polymer supported iminodipropylene glycol functions for removal of boron. React. Funct. Polym. 55 (1), 27–33. https://doi.org/10.1016/S1381-5148(02)00196-7.

Tang, Y.P., Chung, T.S., Weber, M., Maletzko, C., 2017a. Development of novel diol-functionalized silica particles toward fast and efficient boron removal. Ind. Eng. Chem. Res. 56 (40), 11618–11627. https://doi.org/10.1021/acs.iecr.7b03115.

Tang, Y.P., Luo, L., Thong, Z., Chung, T.S., 2017b. Recent advances in membrane materials and technologies for boron removal. J. Memb. Sci. 541, 434–446. https://doi.org/10.1016/j.memsci.2017.07.015.

Ting, T.M., Nasef, M.M., Aravindan, D., Ahmad, M.A., Mokhtar, M., Kamarudin, N.A., Anis, F.N.R., 2020. Selective removal of boron from industrial wastewater containing high concentration of ammonia by radiation grafted fibrous adsorbent in fixed bed column. J. Environ. Chem. Eng. 124187. https://doi.org/10.1016/j.jece.2020.104993.

Ting, T.M., Nasef, M.M., Hashim, K., 2016. Evaluation of boron adsorption on new radiation grafted fibrous adsorbent containing N-methyl-D-glucamine. J. Chem. Technol. Biotechnol. 91 (7), 2009–2017. https://doi.org/10.1002/jctb.2016.91.issue-710.1002/jctb.4793.

Uba, Z., Hana, N., Abu, H., Soraya, N., Jumbri, K., Ain, N., Abdullah, F., Abdul, E., Saad, B., 2020. Adsorption of chrysene in aqueous solution onto MIL-88 (Fe) and NH2-MIL-88(Fe) metal-organic frameworks: Kinetics, isotherms, thermodynamics and docking simulation studies. J. Environ. Chem. Eng. 8, 103544.

Wang, B., Guo, X., Bai, P., 2014a. Removal technology of boron dissolved in aqueous solutions – A review. Colloids Surfaces A Physicochem. Eng. Asp. 444, 338–344. https://doi.org/10.1016/j.colsurfa.2013.12.049.

Wang, J., Wang, T., Li, L., Wu, P., Pan, K., Cao, B., 2014b. Functionalization of polyacrylonitrile nanofiber using ATRP method for boric acid removal from aqueous solution. J. Water Process Eng. 3, 98–104. https://doi.org/10.1016/j.jwpe.2014.05.015.

Wang, Z., Ma, K., Zhang, Y., Zhang, X., Ngo, H.H., Meng, J., Du, L., 2021a. High internal phase emulsion hierarchical porous polymer grafting polyol compounds for boron removal. J. Water Process Eng. 41, 102025. https://doi.org/10.1016/j.jwpe.2021.102025.

Wang, Z., Jia, Y., Song, W., Li, X., Xu, K., Wang, Z., 2021b. Optimization of boron adsorption from desalinated seawater onto UiO-66-NH2/GO composite adsorbent using response surface methodology. J. Clean. Prod. 300, 126974. https://doi.org/10.1016/j.jclepro.2021.126974.

Wei, Y.-T., Zheng, Y.-M., Chen, J.P., 2011. Functionalization of regenerated cellulose membrane via surface initiated atom transfer radical polymerization for boron removal from aqueous solution. Langmuir 27 (10), 6018–6025. https://doi.org/10.1021/la200154y.

Wolska, J., Bryjak, M., 2013. Methods for boron removal from aqueous solutions — a review. Desalination 310, 18–24. https://doi.org/10.1016/j.desal.2012.08.003.

Wu, Q., Liu, M., Wang, X., 2019. A novel chitosan based adsorbent for boron separation. Sep. Purif. Technol. 211, 162–169. https://doi.org/10.1016/j.seppur.2018.09.070.

Xu, X., Ding, X.-J., Ao, J.-X., Li, R., Xing, Z., Liu, X.-Y., Guo, X.-J., Wu, G.-Z., Ma, H.-J., Zhao, X.-Y., 2019. Preparation of amidoxime-based PE/PP fibers for extraction of uranium from aqueous solution. Nucl. Sci. Tech. 30 (2). https://doi.org/10.1007/s41365-019-0543-0.

Yao, C., Chen, T., 2017. A film-diffusion-based adsorption kinetic equation and its application. Chem. Eng. Res. Des. 119, 87–92. https://doi.org/10.1016/j.cherd.2017.01.004.

Zerze, H., Karagoz, B., Ozbelge, H.O., Bicak, N., Aydogan, N., Yilmaz, L., 2013. Imino-bis-propane diol functional polymer for efficient boron removal from aqueous solutions via continuous PEUF process. Desalination 310, 158–168. https://doi.org/10.1016/j.desal.2012.07.013.